

# The Kerr-de Sitter Universe

Sarp Akcay  
*University of Southampton\* and  
 University of Texas at Austin*

Richard A. Matzner  
*Center for Relativity, University of Texas at Austin  
 Texas Cosmology Center, University of Texas at Austin †*

It is now widely accepted that the universe as we understand it is accelerating in expansion and fits the de Sitter model rather well. As such, a realistic assumption of black holes must place them on a de Sitter background and not Minkowski as is typically done in General Relativity. The most astrophysically relevant black hole is the uncharged, rotating Kerr solution, a member of the more general Kerr-Newman metrics. A generalization of the rotating Kerr black hole to a solution of the Einstein's equation with a cosmological constant  $\Lambda$  was discovered by Carter [1]. It is typically referred to as the Kerr-de Sitter spacetime. Here, we discuss the horizon structure of this spacetime and its dependence on  $\Lambda$ . We recall that in a  $\Lambda > 0$  universe, the term 'extremal black hole' refers to a black hole with angular momentum  $J > M^2$ . We obtain explicit numerical results for the black hole's maximal spin value and get a distribution of admissible Kerr holes in the  $(\Lambda, \text{spin})$  parameter space. We look at the conformal structure of the extended spacetime and the embedding of the 3-geometry of the spatial hypersurfaces. In analogy with Reissner-Nordström -de Sitter spacetime, in particular by considering the Kerr-de Sitter causal structure as a distortion of the Reissner-Nordström-de Sitter one, we show that spatial sections of the extended spacetime are 3-spheres containing 2-dimensional topologically spherical sections of the horizons of Kerr holes at the poles. Depending on how a  $t = \text{constant}$  3-space is defined these holes may be seen as black or white holes (four possible combinations).

## I. INTRODUCTION

The WMAP results of the last decade ([2], [3], [4], [5]) have confirmed the current cosmological paradigm: that our universe is given by the  $\Lambda$ CDM model with the dark energy component equivalent to a cosmological "constant"  $\Lambda > 0$  making up almost three quarters of its total energy content ( $0.728 \leq \Omega_\Lambda \leq 0.738$  according to latest analysis in [2]). The first indication of a dark energy component was obtained in 1998 when type Ia supernovae data were analyzed and pointed toward an accelerating expansion of the universe ([6], [7]). While  $\Lambda$  made a negligible contribution to the total energy density of the early universe, the energy density of all other components (matter, cold dark matter, radiation, neutrinos and gravitational waves) decreases as the universe expands, so  $\Lambda$  became (at some point in the past) the dominant term in the total energy density. In the distant future, the other components will be several orders of magnitude smaller in density than  $\Lambda$ , thus they will become negligible. In this final state, the energy-momentum will be completely given by:

$$T_{\mu\nu} = \Lambda g_{\mu\nu}. \quad (1)$$

The spatially homogeneous cosmological solution to Einstein's equation ( $G_{\mu\nu} = 8\pi T_{\mu\nu}$ ) with this constant  $\Lambda$  as the source term is the de Sitter (dS) spacetime. First discovered by de Sitter in 1916 ([8], [9], [10]), the de Sitter metric describes an empty universe whose expansion is ever accelerating as time rolls forward. It is best visualized as a 4-dimensional hyperboloid (see [11] for nice illustrations)

$$-X_0^2 + X_1^2 + X_2^2 + X_3^2 + X_4^2 = r_C^2 \quad (2)$$

embedded in 5-dimensional flat Minkowski spacetime

$$ds^2 = -dX_0^2 + dX_1^2 + dX_2^2 + dX_3^2 + dX_4^2. \quad (3)$$

---

\*Electronic address: sa18g09@soton.ac.uk

†Electronic address: matzner2@physics.utexas.edu

To visualize the geometry of de Sitter spacetime in four dimensions, we perform a coordinate transformation from  $(X_0, X_1, X_2, X_3, X_4)$  to  $(T, \chi, \theta, \phi)$  coordinates that satisfy Eq.(2). The transformation equations are

$$\begin{aligned} r_C \sinh(T/r_C) &= X_0, & r_C \cosh(T/r_C) \cos \chi &= X_1, \\ r_C \cosh(T/r_C) \sin \chi \cos \theta &= X_2, & r_C \cosh(T/r_C) \sin \chi \sin \theta \cos \phi &= X_3, \\ r_C \cosh(T/r_C) \sin \chi \sin \theta \sin \phi &= X_4, \end{aligned} \quad (4)$$

where  $0 \leq \chi, \theta \leq \pi$  and  $0 \leq \phi \leq 2\pi$ .  $r_C$  is a cosmological length scale that equals  $\sqrt{3/\Lambda}$  (often referred to as the Hubble length). With these substitutions, the de Sitter metric as given by Eq.(3) becomes [11], [12]

$$ds^2 = -dT^2 + r_C^2 \cosh^2(T/r_C) [d\chi^2 + \sin^2 \chi (d\theta^2 + \sin^2 \theta d\phi^2)] . \quad (5)$$

As can be seen from the metric of Eq.(5), the geometry of de Sitter spacetime is that of a 3-sphere which contracts to a minimum size at  $T = 0$  and then expands hyperbolically in time. The coordinates  $(T, \chi, \theta, \phi)$  are called the global coordinates of de Sitter spacetime because they cover the entire 4-dimensional spacetime manifold. The  $T = \text{constant}$  surfaces are 3-spheres of constant positive curvature.

There are other choices for coordinates in dS spacetime. One such system of coordinates  $(\hat{t}, \hat{x}, \hat{y}, \hat{z})$  is the so-called *conformally flat* ([11]) slicing of the 4-dimensional hyperboloid given by the following relations:

$$\hat{t} = r_C \ln \left( \frac{X_0 + X_1}{r_C} \right), \quad \hat{x} = \frac{r_C X_2}{X_0 + X_1}, \quad \hat{y} = \frac{r_C X_3}{X_0 + X_1}, \quad \hat{z} = \frac{r_C X_4}{X_0 + X_1}, \quad (6)$$

which give us the following for the de Sitter metric

$$ds^2 = -d\hat{t}^2 + e^{2\hat{t}/r_C} (d\hat{x}^2 + d\hat{y}^2 + d\hat{z}^2) . \quad (7)$$

Note that  $\hat{t} = \text{constant}$  hypersurfaces are flat in this coordinate system. However, because  $\hat{t}$  is ill-defined for  $X_0 + X_1 \leq 0$ , the conformal coordinates cover only half of the hyperboloid.

Finally, we can choose to use another set of coordinates  $(t, r, \theta, \phi)$  given by the following [11], [12]:

$$\begin{aligned} X_0 &= \sqrt{r_C^2 - r^2} \sinh t/r_C, & X_1 &= \sqrt{r_C^2 - r^2} \cosh t/r_C, \\ X_2 &= r \sin \theta \cos \phi, & X_3 &= r \sin \theta \sin \phi, & X_4 &= r \cos \theta . \end{aligned} \quad (8)$$

This set of coordinates is known as *static coordinates* because of the particular form that the dS metric acquires:

$$ds^2 = - \left( 1 - \frac{\Lambda}{3} r^2 \right) dt^2 + \frac{dr^2}{1 - \frac{\Lambda}{3} r^2} + r^2 (d\theta^2 + \sin^2 \theta d\phi^2) . \quad (9)$$

Clearly,  $t = \text{constant}$  slices in this coordinate system are invariant under time translations and reversals. In other words, the 3-geometry of the hypersurfaces is constant in time i.e. *static*. As can be seen from the right hand panel of Fig. 1, there is clearly a null boundary in the static slicing of de Sitter spacetime. Physically, this null surface corresponds to the cosmological horizon of de Sitter spacetime (where the expansion rate of spacetime exceeds the speed of light). This horizon is located at  $r = r_C$  where  $r_C$  is the root of  $g_{rr}^{-1} = 0$  given in Eq.(9):  $r_C = \sqrt{3/\Lambda}$ . This is the same  $r_C$  as the one in Eqs.(2) — (8). Although the significance of  $r_C$  as a horizon only becomes apparent in static coordinates, it clearly is the cosmological characteristic length scale for de Sitter spacetime in all coordinate systems. Static coordinates are especially relevant since the Kerr-de Sitter metric is usually presented in terms of them, and the horizon structure of the Kerr-de Sitter spacetime is most transparent in these coordinates.

There has been a sporadic influx of interest on the Kerr-de Sitter solution since the 1970s. Most of this has been in the context of singularity theorems, string theory (mostly focused on Kerr-Anti-de Sitter) and trying to come up with physical interpretations for solutions to Einstein equation with three or more parameters. In this article, we provide a clear and concise introduction to this special solution. We also present numerical results that quantify the properties of Kerr black holes in this spacetime. We show that in a  $\Lambda > 0$  universe, the black hole spin can exceed the  $a = M$  bound and that for  $\Lambda > 1/9M^{-2}$  non-rotating black holes cannot exist. Finally, we clarify and provide some foundations for understanding what may be a well known but not so well grasped peculiarity of Reissner-Nordström-de Sitter and Kerr-de Sitter solutions: The time reversal of the evolution neighboring regions that are separated by the null horizon  $r_C$ . Although this time reversal is often mentioned in the literature, how it comes about has hardly ever been explained.

The remainder of the paper is organized as follows. In Section II we introduce Schwarzschild-de Sitter spacetime. This is our ‘warm-up’ cosmological model for Kerr-de Sitter. In section III, we present a thorough study of the

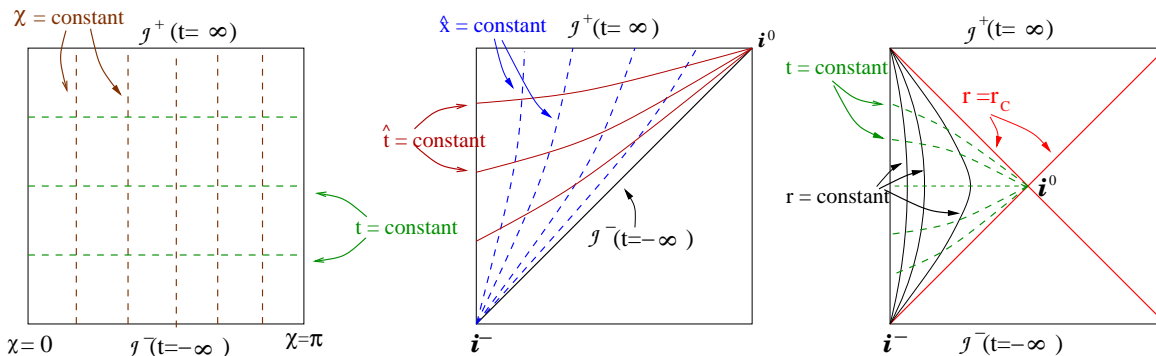


FIG. 1: de Sitter spacetime presented in three different coordinate systems. From left to right, we have the Penrose diagrams with global, hyperbolic and static coordinates. As can be seen in the figure, global coordinates cover the entire manifold whereas static coordinates only cover a quarter of it.  $\mathcal{J}^\pm$  represent future(+) and past (-) null infinities. A peculiar property of de Sitter spacetime is that null future infinities  $\mathcal{J}^\pm$  can be spacelike surfaces [11] where all timelike and null lines end up.  $i^-$ ,  $i^0$  represent past timelike ( $0 \leq r \leq r_C$ ) and spacelike infinities, respectively (see [11], chapter 5).

Kerr-de Sitter universe and present its peculiar properties. One of these is the possibility that the black hole spin parameter  $a$  may exceed the black hole mass parameter  $M$ . An extreme Kerr black hole in Kerr-de Sitter will have  $a > M$ ; we provide numerical examples in section III. In section IV, we will investigate the conformal structure of the Kerr-de Sitter universe and the extended spacetime. We extend the correspondence between Reissner-Nordström-de Sitter (RNdS) and Kastor-Traschen (KT) spacetimes to an approximate correspondence between Kerr-de Sitter and KT spacetimes. With this we show that the extended Kerr-de Sitter spacetime can be physically interpreted as a 3-sphere containing a Kerr hole and a counter-rotating Kerr hole located antipodally from one another. Thus the Kerr-de Sitter spacetime can be extended to two holes analogously to the extension of the charged RNdS case (first interpreted to represent two oppositely charged holes in [14]).

## II. SCHWARZSCHILD-DE SITTER UNIVERSE

Schwarzschild-de Sitter (SdS) spacetime is a spherically symmetric uncharged black hole solution to Einstein's equation with the cosmological constant  $\Lambda$  as the source term (Eq.(1)) [13], [15], [16], [12]. It is described by two parameters: the black hole mass  $M$  and the cosmological constant  $\Lambda$ . Both of these parameters are taken to be positive in order to obtain the SdS solution. In static coordinates, the SdS metric is given by the following expression [17]:

$$ds^2 = - \left( 1 - \frac{2M}{r} - \frac{\Lambda r^2}{3} \right) dt^2 + \frac{dr^2}{\left( 1 - \frac{2M}{r} - \frac{\Lambda r^2}{3} \right)} + r^2 d\Omega_2^2, \quad (10)$$

where  $d\Omega_2^2$  is the metric on a 2-sphere. To determine the position of the event horizon(s) in this spacetime, we must find where the expansion,  $\Theta_{(\ell)}$ , of the outgoing null geodesics  $\ell^\mu$  equals zero. Technically speaking, this method gives the locations of the apparent horizons, but since the spacetime is static, the apparent and the event horizons coincide. A quick computation (see Appendix A2 in [18] for details) shows that the expansion is proportional to  $g_{rr}^{-1}$  of Eq.(10). So, the roots of

$$g_{rr}^{-1} = 1 - \frac{2M}{r} - \frac{\Lambda r^2}{3} = 0 \quad (11)$$

give us the locations of the horizons in this spacetime. This equation is a truncated cubic which generally yields three complex roots. The condition for all three roots to be real is  $9M^2\Lambda < 1$  ( $\Lambda = (9M^2)^{-1}$  corresponds to the degenerate horizon case where two real roots coincide). Even with this condition, only two of these three roots are positive. Physically, the smaller positive root corresponds to the Schwarzschild black hole horizon  $r_H$  and the larger root to the cosmological horizon  $r_C$ . The explicit expressions for the roots can be presented in the following form [19] (also

see [36] and its Fig.1):

$$\begin{aligned} r_1 &= \frac{2}{\sqrt{\Lambda}} \cos \frac{\theta}{3}, \\ r_2 &= \frac{2}{\sqrt{\Lambda}} \cos \left[ \frac{\theta}{3} + \frac{2\pi}{3} \right], \\ r_3 &= \frac{2}{\sqrt{\Lambda}} \cos \left[ \frac{\theta}{3} + \frac{4\pi}{3} \right], \end{aligned}$$

where  $\theta$  is defined by  $\cos \theta = -3\sqrt{\Lambda}M$ . With the reality condition  $9M^2\Lambda < 1$ ,  $0 \geq \cos \theta > -1$  for  $M, \Lambda \geq 0$ . Thus, we have  $\pi/2 < \theta < \pi$ . In this range for  $\theta$ , the positive roots are  $r_1$  and  $r_3$  with  $r_3 < r_1$ ;  $r_2$  is negative. So,  $r_3$  is the black hole horizon  $r_H$  and  $r_1$  is the de Sitter horizon  $r_C$ . The reality condition has the physical interpretation of imposing an upper mass limit  $M_{max} = \Lambda^{-1/2}/3$  on the Schwarzschild black hole; in other words, requiring that the black hole radius  $r_H$  be roughly smaller than the size of the de Sitter horizon  $r_C$ . Obviously, at  $9M^2\Lambda = 1$  i.e.  $M = M_{max}$ , the two horizons coincide ( $r_H = r_C = \Lambda^{-1/2}$ ).

The details of how one obtains the conformal structure of SdS spacetime can be found in [19]. The Penrose-Carter diagram for the SdS spacetime [20] is displayed in the lower-left panel of Fig. 2. Unlike in Schwarzschild spacetime, two separate coordinate charts are needed to cover the SdS spacetime. One proceeds by introducing Kruskal type null coordinates in the vicinity of the black hole horizon and Hawking-Gibbons coordinates [20] in the vicinity of the cosmological horizon. Furthermore, there are now infinitely many regions where the Killing vector  $\partial/\partial t$  is timelike as opposed to only two regions in regular Schwarzschild spacetime. There is an infinite sequence of singularities  $r = 0$  and spacelike infinities  $r = \infty$  in the conformal representation of SdS universe. So, on any spacelike hypersurface that we may pick in this extended spacetime, we would get a picture similar to that of an infinite number of beads on a wire. However, in this case, the beads are actually connected (but not causally) by throats of different sizes, which depend on how far into the black hole region ( $r < r_H$ ) a hypersurface crosses. The same goes for the maximum radii of the beads as a given hypersurface can go arbitrarily far beyond  $r = r_C$  before ‘exiting’ through the companion cosmological horizon. We illustrate the geometries of two different hypersurfaces in the upper-right portion of Fig. 2.

Furthermore, the ‘color’ of the ‘black’ hole that one observes is determined by where the observer’s spacelike slice intersects a given horizon  $r_H$ . Depending on the location of the intersection points, one may end up with any one of the following four combinations for the two trapped regions: *Black Hole* (BH) – BH, *White Hole* (WH) – WH, BH – WH, WH – BH (We define a BH to be a the region inside a future event horizon; a WH as the region inside a past event horizon). The various pairings between BHs and WHs are shown in the lower-right panel of Fig. 2 where we slice the  $r_H < r < r_C$  region of spacetime with four different hypersurfaces extending from one hole to the next.

### III. KERR-DE SITTER SPACETIME

The solution to Einstein’s equation with cosmological constant describing a black hole with spin  $a$  is called the Kerr-de Sitter (KdS) solution. It was found by Carter and was first published in the 1973 *Les Houches* lectures edited by DeWitt & DeWitt [1]. Later, it was discovered that this solution is a special case of the general Plebański-Demiański family of metrics [21], [22], [23], [24]. The Plebański-Demiański solution is the most general solution for a Petrov Type D spacetime. Kerr-de Sitter happens to be a very restricted case of the general Plebanský-Demianský solution with zero NUT charge, acceleration, electric and magnetic charges. In the Boyer-Lindquist like coordinates used by Carter, the Kerr-de Sitter metric is as follows

$$\begin{aligned} ds^2 &= (r^2 + a^2 \cos^2 \theta) \left[ \frac{dr^2}{\Delta_r} + \frac{d\theta^2}{1 + \frac{\Lambda}{3} a^2 \cos^2 \theta} \right] + \sin^2 \theta \frac{1 + \frac{\Lambda}{3} a^2 \cos^2 \theta}{(r^2 + a^2 \cos^2 \theta)} \left[ \frac{adt - (r^2 + a^2)d\phi}{1 + \frac{\Lambda}{3} a^2} \right]^2 \\ &\quad - \frac{\Delta_r}{(r^2 + a^2 \cos^2 \theta)} \left[ \frac{dt - a \sin^2 \theta d\phi}{1 + \frac{\Lambda}{3} a^2} \right]^2, \end{aligned} \quad (12)$$

where

$$\Delta_r = (r^2 + a^2) \left( 1 - \frac{\Lambda}{3} r^2 \right) - 2Mr = r^2 - 2Mr + a^2 - \frac{\Lambda r^2}{3} (r^2 + a^2). \quad (13)$$

The constant  $\Lambda$  has the opposite sign here compared to Carter’s original version in [1]; Hawking & Gibbons [20] agree with our choice of sign for de Sitter. This choice of sign is consistent with our sign of  $\Lambda$  for SdS metric (see Eq.(10)). As is well known, the  $a \rightarrow 0, M \neq 0$  limit of KdS is SdS.

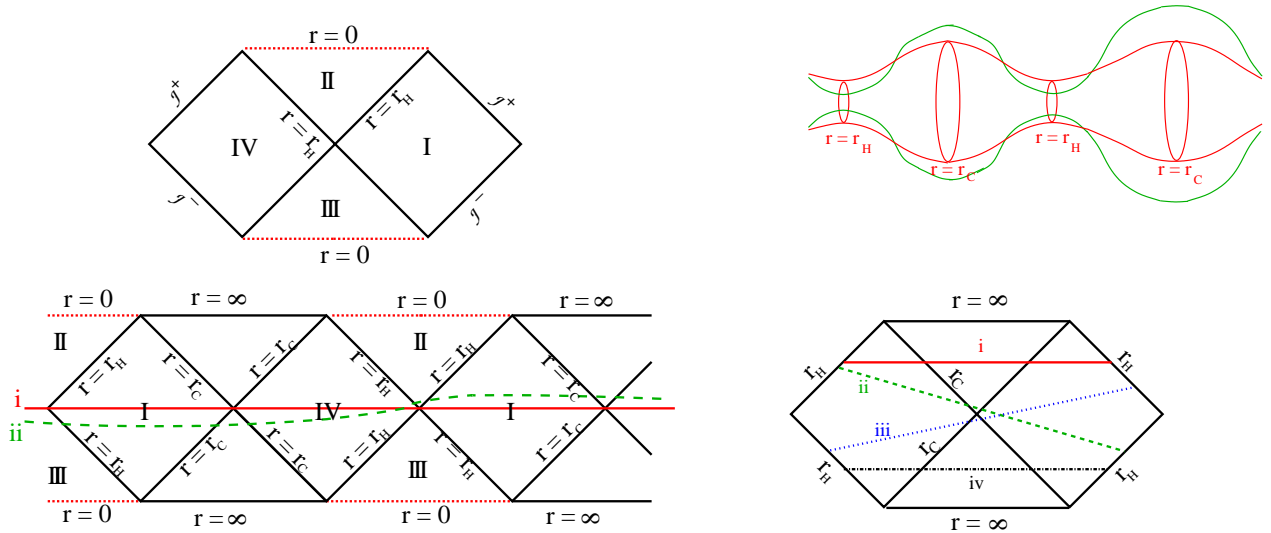


FIG. 2: The Penrose diagrams for Schwarzschild (upper-left) and Schwarzschild-de Sitter (lower-left) spacetimes. The bottom diagram continues ad infinitum to the right and to the left with infinitely many curvature singularities ( $r = 0$ ) and spacelike infinities ( $r = \infty$ ).  $\mathcal{J}^\pm$  label the future and past null infinities. Region I in SdS spacetime is analogous to region I of Schwarzschild spacetime where the Killing vector  $\partial/\partial t$  is timelike and future directed. It is timelike, but past directed in region IV and spacelike in regions II and III. The horizontal solid/red (labelled i) curve is a time-symmetric cut of the spacetime, whereas the dashed/green (ii) curve represents a more generic spacelike hypersurface. The “beads on a string” on the upper-right of the figure show the geometry along hypersurfaces i and ii. Of course, there is no string, but simply black/white hole throats connecting (not causally) each bead universe to the next. Finally in the lower-right panel, we slice a 2-hole, 1-bead section of the SdS spacetime to illustrate the different scenarios involving white/black holes in the 3-geometry of the hypersurfaces. We pick 4 different hypersurfaces: red, solid (i); green, dashed (ii); blue, dotted (iii); black, dash-triple-dotted (iv). These slicings respectively give  $BH - BH$ ,  $BH - WH$ ,  $WH - BH$ ,  $WH - WH$  within the chosen hypersurface.

We will write Eq.(12) in a more compact form:

$$ds^2 = \rho^2 \left[ \frac{dr^2}{\Delta_r} + \frac{d\theta^2}{\Delta_\theta} \right] + \frac{\Delta_\theta \sin^2 \theta}{\rho^2} \left[ a \frac{dt}{\Xi} - (r^2 + a^2) \frac{d\phi}{\Xi} \right]^2 - \frac{\Delta_r}{\rho^2} \left[ \frac{dt}{\Xi} - a \sin^2 \theta \frac{d\phi}{\Xi} \right]^2, \quad (14)$$

where

$$\begin{aligned} \Delta_\theta &= 1 + \frac{\Lambda}{3} a^2 \cos^2 \theta, \\ \rho^2 &= (r^2 + a^2 \cos^2 \theta), \\ \Xi &= 1 + \frac{\Lambda}{3} a^2. \end{aligned} \quad (15)$$

Carter included the factor of  $\Xi$  to ensure that there are no conical singularities on the spatial axis  $\theta = \{0, \pi\}$ . We show the details of how this works in appendix A. If desired, one can rescale the Boyer-Lindquist time coordinate  $t$  by a factor of  $\Xi^{-1}$ ; the version of the KdS metric presented in [31] indeed embodies this slight modification.

To see that this is indeed asymptotically de Sitter, consider the  $M = 0$  limit of Eq.(12):

$$\begin{aligned} ds^2 &= (r^2 + a^2 \cos^2 \theta) \left[ \frac{dr^2}{(r^2 + a^2)(1 - \Lambda r^2/3)} + \frac{d\theta^2}{1 + \frac{\Lambda}{3} a^2 \cos^2 \theta} \right] \\ &+ \sin^2 \theta \frac{1 + \frac{\Lambda}{3} a^2 \cos^2 \theta}{(r^2 + a^2 \cos^2 \theta)} \left[ \frac{adt - (r^2 + a^2)d\phi}{1 + \frac{\Lambda}{3} a^2} \right]^2 \\ &- \frac{(r^2 + a^2)(1 - \Lambda r^2/3)}{(r^2 + a^2 \cos^2 \theta)} \left[ \frac{dt - a \sin^2 \theta d\phi}{1 + \frac{\Lambda}{3} a^2} \right]^2. \end{aligned} \quad (16)$$

It is not so obvious from Eq.(16) that what one has is regular de Sitter spacetime. This is because Carter’s Boyer-Lindquist type coordinates need to be “untwisted” in order for us to really see that Eq.(16) gives the dS metric. The

untwisting is realized by the following coordinate transformation:

$$\begin{aligned} T &= t/\Xi, & \bar{\phi} &= \phi - a\Lambda t/3\Xi, \\ y \cos \Theta &= r \cos \theta, \\ y^2 &= \frac{1}{\Xi} [r^2 \Delta_\theta + a^2 \sin^2 \theta]. \end{aligned} \quad (17)$$

By doing the algebra, one can show that these coordinate transformations yield the usual form of the de Sitter metric in  $(T, y, \Theta, \bar{\phi})$  coordinates:

$$ds_{dS}^2 = -(1 - \Lambda y^2/3)dT^2 + \frac{1}{1 - \Lambda y^2/3}dy^2 + y^2(d\Theta^2 + \sin^2 \Theta d\bar{\phi}^2). \quad (18)$$

It is also interesting to note that one can cast the KdS spacetime into a Kerr-Schild like form. In general, the Kerr-Newman vacuum solution to Einstein's equation can be written in a special form called the Kerr-Schild form of the metric. This form is given by ([25],[26], [32], [33]),

$$g_{\mu\nu} = \eta_{\mu\nu} + 2Hk_\mu k_\nu, \quad (19)$$

where  $H$  is a function of spacetime coordinates and for the Kerr solution is proportional to the constant  $M$ :  $H = 2Mr/\rho^2$ .  $\eta_{\mu\nu}$  is the Minkowski metric of flat spacetime and  $k^\mu$  is a null vector with respect to both  $g_{\mu\nu}$  and  $\eta_{\mu\nu}$ . Of course, here we are not dealing with the Minkowski metric; the  $M \rightarrow 0$  limit of Kerr-de Sitter metric is simply the de Sitter metric as was shown above. But in analogy to Eq.(19), we write

$$ds^2 = ds_0^2 + H(k_\mu dx^\mu)^2, \quad (20)$$

where  $H = 2Mr/\rho^2$  and  $ds_0^2$  is the background de-Sitter metric. We can express this background in Kerr-Schild (KS) coordinates  $(\tau, r, \theta, \Phi)$ :

$$ds_0^2 = -\frac{\Delta_\theta}{\Xi}(1 - \Lambda r^2/3)d\tau^2 + \frac{\rho^2}{(r^2 + a^2)(1 - \Lambda r^2/3)}dr^2 + \frac{\rho^2}{\Delta_\theta}d\theta^2 + \frac{r^2 + a^2}{\Xi}\sin^2 \theta d\Phi^2. \quad (21)$$

The null vector equals

$$k_\mu dx^\mu = \frac{\Delta_\theta}{\Xi}d\tau + \frac{\rho^2}{(r^2 + a^2)(1 - \Lambda r^2/3)}dr - \frac{a \sin^2 \theta}{\Xi}d\Phi. \quad (22)$$

The coordinate transformation that connects KS and BL coordinates is given in [31] and is as follows:

$$d\tau = dt + \frac{2Mr}{(1 - \Lambda r^2/3)\Delta_r}dr, \quad d\Phi = d\phi - \frac{\Lambda}{3}adt + \frac{2Mr}{(r^2 + a^2)\Delta_r}dr. \quad (23)$$

Applying this coordinate transformation to obtain Carter's form of the KdS metric in BL coordinates (Eq.(14)) is somewhat tedious, but straightforward. At first, the resulting metric in BL coordinates  $(t, r, \theta, \phi)$  appears to be different:

$$\begin{aligned} ds^2 &= -\frac{\Delta_\theta}{\Xi}(1 - \Lambda r^2/3)dt^2 + \frac{2Mr}{\rho^2} \left[ dt - \frac{a \sin^2 \theta}{\Xi}d\phi \right]^2 \\ &\quad + \frac{r^2 + a^2}{\Xi} \sin^2 \theta \left( d\phi - \frac{\Lambda a}{3}dt \right)^2 + \frac{\rho^2}{\Delta_r}dr^2 + \frac{\rho^2}{\Delta_\theta}d\theta^2. \end{aligned} \quad (24)$$

However, with a little work, one can show that this is indeed Carter's metric (Eq.(12) with the one difference in the scaling of the time coordinate by a factor of  $\Xi = 1 + \Lambda a^2/3$ .

We are interested in understanding the horizon structure of this spacetime. We look for the locations of the apparent horizons in the same way that we have done in section II. First, we find the principal null vectors  $(\ell^\mu, n^\mu)$  of the spacetime. The Plebański-Demiański metrics are of Petrov Type D, which means that there are only two principal null vectors [25], [22]. The  $\ell^\mu$  and  $n^\mu$  are defined only up to an overall functional factor; we impose the standard relative normalization  $\ell_\mu n^\mu = -1$ , which still allows for a scaling of  $\ell^\mu$  with an inverse scaling of  $n^\mu$ . We then compute the expansion of the outgoing null rays  $\ell^\mu$  on the 2-surface that is transverse to the 1+1 dimensional spacetime spanned by  $\ell^\mu$  and  $n^\mu$ ; where this expansion equals zero is the location of the apparent horizon. Mathematically speaking, we



solve  $\Theta_{(\ell)} \equiv q^\mu_\nu \nabla_\mu \ell^\nu = 0$  with the metric of the transverse 2-surfaces given by  $q_{\mu\nu} = g_{\mu\nu} + (\ell_\mu n_\nu + n_\mu \ell_\nu)/(-\ell_\alpha n^\alpha)$ . For KdS spacetime, in Carter's BL type coordinates, the outgoing null vector  $\ell^\mu$  is

$$\ell^\mu = \sqrt{\frac{\Delta_r}{2\rho^2}} \left( \frac{r^2 + a^2}{\Delta_r} \Xi, 1, 0, \frac{a}{\Delta_r} \Xi \right). \quad (25)$$

Notice that  $\ell^\mu$  is a Killing vector of the spacetime. For the expansion, we obtain

$$\Theta_{(\ell)} \propto 3r \Delta_r. \quad (26)$$

Here, we deliberately left out coefficients (all positive) that tell us nothing about the location of apparent horizons (where  $\Theta_{(\ell)} = 0$ ).

$$\begin{aligned} \Theta_{(\ell)} = 0 \quad \text{where} \quad \Delta_r = 0; \\ (r^2 + a^2)\left(1 - \frac{\Lambda}{3}r^2\right) - 2Mr = 0; \\ (r - r_+)(r - r_-)(r - r_C)(r - r_{--}) = 0. \end{aligned} \quad (27)$$

Here,  $r_\pm$  are the Kerr black hole horizons, and  $r_C$  is the cosmological horizon.  $r_{--} < 0$  is another cosmological horizon "inside" the singularity at  $r = 0$ . Eq.(27) yields four real roots only for certain values of  $\Lambda = \Lambda(M, a)$  or  $M = M(a, \Lambda)$ . To determine what the limiting values are, we impose the restriction on the quartic formula [28] that all four roots be real. This translates to an upper bound for  $M$  that we call  $M_{max}$  which is determined by the following equation:

$$\left[ \frac{1}{\Lambda} \left( 1 - \frac{\Lambda}{3} a^2 \right) - 4a^2 \right]^3 = \frac{1}{\Lambda} \left[ \left( 1 - \frac{\Lambda}{3} a^2 \right) \left[ \frac{1}{\Lambda} \left( 1 - \frac{\Lambda}{3} a^2 \right)^2 + 12a^2 \right] - 18M_{max}^2 \right]^2. \quad (28)$$

Only for  $M < M_{max}$  do we get three distinct positive roots for  $\Delta_r$ , which give us the two black hole horizons  $r_\pm$  and the cosmological horizon  $r_C$ . Eq.(28) is rather complicated to solve analytically without assigning specific values for  $M$  and  $a$ . However, we can at least check this condition at the  $a = 0$  limit, which gives

$$M < M_{max} = \frac{1}{3\sqrt{\Lambda}}, \quad (29)$$

agreeing with the Schwarzschild-de Sitter result. From a physical perspective, one sees that an upper bound on the black hole mass  $M$  simply reflects the fact that since the cosmology induces a relative recession speed between two radially separated points that increases with distance, the horizon of a larger black hole would be torn apart by the cosmic expansion.

We prefer not to display the solutions for the roots of  $\Delta_r$  explicitly, since writing down the solutions of a quartic equation using the quartic formula is not always enlightening. By assigning values to the black hole's mass  $M$  and spin  $a$ , we can make the solutions to the quartic equation look less crowded without loss of generality. For simplicity, we set  $M$  equal to 1 and scale the values for  $a$  and  $\Lambda$  accordingly (recall that  $\Lambda$  has dimensions of  $(\text{length})^{-2}$ ). A very interesting case is determining the horizon locations for Kerr when  $a = M$ . One would naively expect that the black hole roots  $r_-$  and  $r_+$  meet at a single location as this is the case in Kerr spacetime. But plotting this quartic function in the proper range for  $\Lambda$  shows that the function still possesses three separate, positive roots. Solving Eq.(28) for  $\Lambda_{max}$  with  $a = M$  yields

$$\tilde{\Lambda}_{max} \approx 0.1528377, \quad (30)$$

where we have introduced the dimensionless cosmological constant  $\tilde{\Lambda} \equiv M^2 \Lambda$ . Similarly, for the spin,  $\tilde{a} \equiv a/M$  and radial distance  $\tilde{r} \equiv r/M$ . At  $\Lambda = \Lambda_{max}$ , the outer roots  $r_+$  and  $r_C$  merge, which physically corresponds to what is called *the extreme (or marginal) naked singularity case* in [29]. The double root is a degenerate cosmological horizon and the smaller root  $r_-$  is the usual Cauchy horizon. Any value we pick for  $\tilde{\Lambda}$  less than  $\tilde{\Lambda}_{max} \approx 0.1528377$  should give us an asymptotically de Sitter spacetime with a regular Kerr black hole in it. Let us pick  $\tilde{\Lambda} = 0.1$  for example (This should read  $\Lambda M^2 = 0.1$  if we restore the dimensions). Solving the quartic for  $\Delta_r$  explicitly with  $M = a$  and  $\tilde{\Lambda} = 0.1$  yields *three* positive roots (not two) to

$$\Delta_r = r^2 - 2r + 1 - \frac{0.1}{3} r^2 (r^2 + 1) = 0, \quad (31)$$

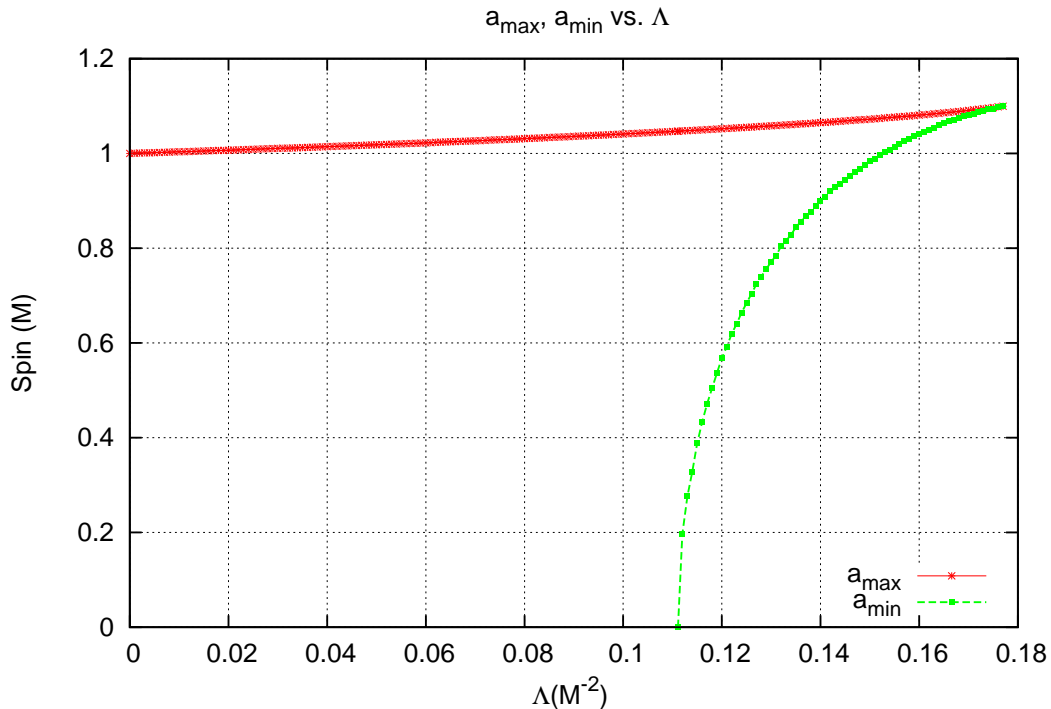


FIG. 3: Plot of  $a_{max}$  and  $a_{min}$  versus  $\Lambda$  with the black hole mass  $M = 1$ . The upper, solid (red) curve (\* marks) represents  $a_{max}$  for a KdS black hole. Note that  $a_{max} > M$  for all values of  $\Lambda > 0$  and  $a_{max} = M$  only for the asymptotically flat Kerr case ( $\Lambda = 0$ ). The lower, dotted (green) curve (square marks) represents  $a_{min}$ , the minimum spin value the black hole needs to have in order to preserve its horizon structure.  $a_{min}$  becomes non-zero only for values of  $\tilde{\Lambda}$  greater than  $1/9 = 0.11\overline{111}$  (the Schwarzschild-de Sitter limit). The two curves meet at the maximum value of  $\tilde{\Lambda} = 0.1778/M^2$ . For  $\Lambda > \tilde{\Lambda}$  there is no black hole, but only a naked singularity. The ultimate extremal spin value at  $\Lambda = \tilde{\Lambda}$  equals  $\tilde{a} \approx 1.10084M$ .

which are

$$\tilde{r}_- \approx 0.8097645665, \quad \tilde{r}_+ \approx 1.485880984, \quad \tilde{r}_C \approx 3.975723107. \quad (32)$$

Clearly, the  $r_{\pm}$  are far from merging for this value of  $\Lambda$ , which tells us that the  $a = M$  value no longer represents the extremal Kerr black hole. Since we know that the  $\Lambda \rightarrow 0$  limit of KdS is regular Kerr spacetime, if we pick a much smaller value for  $\Lambda$ , we should get  $r_- \approx r_+$ . For example, for  $\tilde{\Lambda} = 10^{-4}$ , one gets

$$\tilde{r}_- \approx 0.9919334965, \quad \tilde{r}_+ \approx 1.008266559.$$

These numerical results are simply counter-examples showing that  $a = M$  case does not yield an extremal Kerr black hole in Kerr-de Sitter spacetime. Then, what value of  $a = a_{max}$  makes the black hole extremal? For extremality, the black hole horizons should coincide i.e.  $r_+ = r_-$ . This implies that the surface gravity  $\kappa$  of the Kerr-de Sitter black hole equals zero. Since  $r_{\pm}$  are roots of  $\Delta_r$ , a fourth-order polynomial in  $r$ , the only way one can have  $r_+ = r_-$  is if the two roots merge at a local extremum of  $\Delta_r$ . Thus, the following condition needs to be satisfied at  $a = a_{max}$ :

$$\partial_r \Delta_r(r = r_{\pm}) = 0. \quad (33)$$

Since  $a_{max}$  depends on  $\Lambda$ , we proceed by first specifying a value for  $\Lambda$  (setting up the cosmology) then solving the  $\Delta_r = 0$  quartic equation (Eq.(27)) for the middle two roots  $r_-$  and  $r_+$ . At this point, since the spin  $a$  is at a given arbitrary initial value, we do not expect that  $r_+ = r_-$ . To ensure this, we evaluate  $\partial_r \Delta_r|_{r=r_{\pm}}$  using  $a$  as a free parameter. Where this expression equals zero we conclude that the two roots  $r_-$  and  $r_+$  have merged to form an extremum of  $\Delta_r$ ; and as stated above, this only happens at  $a = a_{max}$ . We use standard Newton-Raphson iteration where we input the values for  $M$  and  $\Lambda$  a priori then start with a conservative initial guess for the spin like  $a = 0.99$ . Then we increase  $a$  until we meet the condition in Eq.(33). The final value reached by the numerical run is the maximal spin value  $a_{max}$  that makes the Kerr black hole extremal. For example, for  $\tilde{\Lambda} = 0.1$ , the maximum value



for the spin is  $\tilde{a}_{max} = 1.0409813$  which is slightly above the asymptotically flat Kerr bound  $a = M$ . This means that the black hole can be “overspun” yet still maintain its horizon structure so long as  $a < a_{max}$ . We present the results of a numerical evolution of  $a_{max}$  as a function of  $\Lambda$  in Fig. 3. In the figure, the upper, solid (red) curve represents  $a_{max}$  for a KdS black hole of  $M = 1$  at a given  $\Lambda$ . Note that  $a_{max} > M$  for all values of  $\Lambda > 0$  and we only obtain  $a_{max} = M$  for the pure Kerr case ( $\Lambda = 0$ ). Also in Fig. 3, the lower, dotted (green) curve represents  $a_{min}$ , the minimum spin value the black hole needs to have in order to preserve its double horizon structure. Notice that  $a_{min}$  becomes non-zero only for values of  $\tilde{\Lambda}$  greater than  $1/9 = 0.111\overline{111}$ . The reader will recall that  $1/9$  corresponds to the Schwarzschild-de Sitter limit of  $\Lambda < 1/9M^2$ . So the green curve confirms what we already know: One can not have a non-spinning ( $a = 0$ ) SdS black hole for values of  $\tilde{\Lambda}$  exceeding  $1/9$ . *Thus, if we are to have a black hole in a  $\Lambda > 1/9M^2$  universe, it must be spinning.* This could have interesting consequences on primordial black hole formation scenarios during the inflationary era of the early Universe. If we assume that the cosmology ( $\Lambda$ ) is specified a priori, as it could be during inflation, then we have a minimum spin requirement for the black holes forming during this epoch. This could potentially forbid the formation of Schwarzschild black holes.

Furthermore, as  $\Lambda$  increases, the spin lower bound  $a_{min}$  increases as well, thus shrinking the parameter space of admissible Kerr black holes in a de Sitter background. Once again, there is a physical interpretation for this behavior. As is well known, the Schwarzschild horizon is larger in size than the Kerr horizon of the same mass, so as we consider larger black hole spin, the horizon shrinks in size. As we consider larger  $\Lambda$ , the only black holes that can exist are those with smaller horizons, i.e. larger spin values: thus the need for a Kerr black hole to have a minimum spin value in a de Sitter background. Furthermore, the two curves in Fig. 3 meet at  $\Lambda = \tilde{\Lambda} \approx 0.1778M^{-2}$ , the maximum value of  $\Lambda$  allowing a black hole. If the cosmological constant is any larger than this ultimate value then the black hole can not hold itself together against the cosmic repulsion and simply leaves its place to a naked singularity, although how “naked” this singularity may be is open to debate. This is further discussed in Section V. The extremal spin value  $\bar{a}$  at  $\Lambda = \tilde{\Lambda}$  is also the ultimate value for black hole spin:  $\bar{a} \approx 1.10084M$ .

It is straightforward to verify that  $a_{max}$  represents an extremal Kerr black hole. We do this by computing the surface gravity of the KdS black hole at  $r = r_+$ . As computed explicitly in the appendix B, the surface gravity of the Kerr-de Sitter black hole can be written as follows:

$$\kappa = \frac{1 - \frac{\Lambda}{3}r_+^2}{4Mr_+} \partial_r \Delta_r |_{r=r_+}. \quad (34)$$

(The expression given in [31] looks different, but can be manipulated to exactly equal Eq.(34)). Since by definition an extreme black hole is one where the two horizons (roots of  $\Delta_r$ )  $r_-$  and  $r_+$  meet, one automatically has an extremum of  $\Delta_r$  at that meeting point i.e.  $\partial_r \Delta_r |_{r=r_- = r_+} = 0$ . Thus, the KdS black hole with the doubly degenerate horizon ( $r_- = r_+$ ) is indeed an extremal black hole.

#### IV. GLOBAL STRUCTURE

We start by presenting the Penrose diagram for the Kerr-de Sitter spacetime along the positive z-axis (symmetry axis  $\theta = 0$ ) in Fig.4. Although the Penrose diagrams for Kerr spacetime are usually presented along an equatorial slice ( $\theta = \pi/2$ ), our choice for the spatial cross-section resembles the spherically symmetric Reissner-Nordström-de Sitter more and is also the choice of Hawking & Gibbons in [20]. In fact, the Penrose diagram for KdS looks similar to that of Kerr (cf. [26], [34]) except for the extra horizons at  $r = r_{--}, r_C$  and the fact that conformal infinity,  $\mathcal{I}^+$ , is replaced by a spacelike surface. This is consistent with the spacelike  $\mathcal{I}^+$  also found in de Sitter spacetime ( $\Lambda > 0$ ). Just as in Kerr, one has the black hole event horizon at  $r = r_+$ , the inner black hole [Cauchy] horizon at  $r = r_-$  and a ring singularity at  $r = 0$  which is pictured as the red dashed lines in Fig. 4. But unlike in Kerr, the ring singularity is no longer naked in the region where  $r < 0$ . It is cloaked beyond yet another horizon  $r_{--} < 0$  and past this horizon, there is yet another infinity  $r = -\infty$ . A few words of caution about this diagram: **(1)** The infinities at  $r = \infty$  and  $r = -\infty$  are completely disjointed, **(2)** Technically speaking, the ring singularity lies on the  $\theta = \pi/2$  plane and not on the  $\theta = 0$  cut we are taking, but this somewhat misleading graphical representation of the singularity is standard treatment in the literature whether for Kerr or Kerr-de Sitter spacetimes (cf. [20], [26]).

One can identify different regions of this spacetime. This is indeed what we will do explicitly in this section, first for Reissner-Nordström-de Sitter spacetime then for KdS. The identifications will help reveal the physical picture for these spacetimes: the spatial manifold is a 3-sphere that contains a black/white hole at its antipodal points (poles at  $\chi = 0, \pi$ , see Eq.(5)). Here and henceforth, when we say that a black hole (a 4-dim. object) is contained within a 3-sphere, we mean that its 2-dim. event (or apparent) horizon is centered at the pole of the 3-sphere.

Before continuing with the interpretation of the Kerr-de Sitter Penrose-Carter diagram, we first discuss the Reissner-Nordström-de Sitter (RNdS) ([1]) and Kastor-Traschen (KT) ([35]) solutions. Just as one heavily draws on Reissner-Nordström spacetime to understand the conformal structure of Kerr spacetime, here we will draw on RNdS spacetime

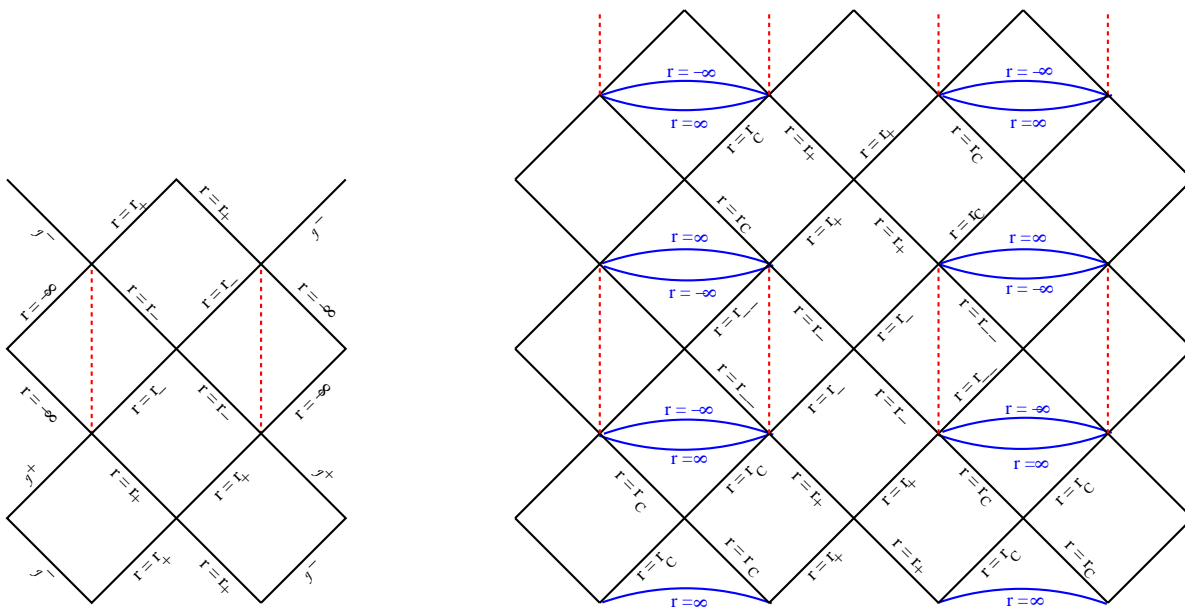


FIG. 4: The Penrose-Carter diagrams for Kerr (left) and Kerr-de Sitter (right) spacetimes along the  $\theta = 0$  cut [20]. When viewed together, the differences between the two spacetimes become obvious. In KdS there are four horizons labelled  $r_{--}$ ,  $r_-$ ,  $r_+$  and  $r_C$ . As in Kerr,  $r_{\pm}$  are the black hole horizons, but there are two extra horizons,  $r_{--}$ ,  $r_C$  which are cosmological in nature. The infinities at  $r = \pm\infty$  are disjoint. The dashed (red) vertical lines represent the curvature singularities at  $r = 0$ . These are actually ring singularities that lie on the  $\theta = \pi/2$  plane. The Kerr singularity is naked when viewed from the region  $r < 0$  whereas in KdS, the same singularity is cloaked behind the horizon  $r_{--}$  for observers at  $-\infty < r < r_{--} < 0$ . The conformal diagram for KdS continues ad infinitum in all directions. As always, the transverse directions ( $\theta, \phi$ ) have been suppressed.

to suggest an interpretation of KdS. We will find that a section of the extended KdS manifold can be interpreted as a 3-sphere containing two counter-rotating Kerr holes: a black hole and a white hole located at antipodal points. A similar interpretation was first mentioned in [14] for the RNdS case; it can be shown in a straightforward manner for the case of “extremal” (charge  $Q$  equaling mass  $M$ ) RNdS spacetime. It turns out that this extremal RNdS spacetime is a single-black-hole Kastor-Traschen spacetime; there is an exact coordinate transformation relating the two solutions. (By construction, the KT solution can accommodate as many black holes as one wishes.) Most of the work on this was done by Brill and collaborators in [29], [30], [41] and throughout this article, we rely on their results repeatedly.

Here, we are mostly interested in the single black hole KT spacetime and its coordinate charts. Nevertheless, we include a brief section on the many black hole KT solution in appendix C for the sake of completeness.

### A. Reissner-Nordström-de Sitter Spacetime

The spherically symmetric, three parameter  $(M, \Lambda, Q)$  solution to Einstein’s equation was also first written down by Carter in [1]. Here  $Q$  represents the electric charge of the black/white hole. The line element for this solution in static coordinates is

$$ds^2 = -f dt^2 + f^{-1} dr^2 + r^2 d\Omega_2^2, \quad (35)$$

where

$$f = f(r) = 1 - \frac{2M}{r} + \frac{Q^2}{r^2} - \frac{\Lambda}{3} r^2, \quad (36)$$

and  $d\Omega_2^2 = d\theta^2 + \sin^2 \theta d\phi^2$  is the metric on the 2-sphere ( $S^2$ ). Once again, the location of the horizons is determined by the roots of the quartic equation  $f = 0$ . As before, only for certain values of  $\Lambda < \Lambda_{max}$ , does one get three real positive roots  $r_- < r_+ < r_C$  representing the inner, outer black hole and the de Sitter horizons. This is what we will refer to as the generic case. There are, of course, non-generic cases where the quartic has only one real positive root or degenerate double or triple roots. These more eccentric cases are mentioned in detail in [29], [30], [41]. Here,

we are concerned with the generic, three positive root case. The Penrose diagram for this case looks exactly like the Penrose diagram displayed for KdS universe in Fig. 4.

For the generic case, where  $f > 0$  and  $r_+ < r < r_C$ , the  $t = \text{constant}$  surfaces are free of singularities. The spatial geometry on such a  $t = \text{constant}$  hypersurface is given by its spatial 3-metric

$$ds_3^2 = f^{-1}dr^2 + r^2d\Omega_2^2. \quad (37)$$

This can be embedded in 4-dimensional Euclidean space  $ds_E^2 = dW^2 + dr^2 + r^2d\Omega_2^2$  by the following definition [29]

$$W \equiv \int \sqrt{f^{-1} - 1} dr. \quad (38)$$

The embedding hypersurface has a minimum radius at the throat of the black hole ( $r = r_+$ ) and maximum radius at the cosmological horizon ( $r = r_C$ ). The spatial topology is  $S^2 \times R^1$ . At this point, let us mention that removing both poles of a 3-sphere changes its topology from  $S^3$  to  $S^2 \times R^1$ , which is the topology of spatial sections of RNdS spacetime. Certainly, hiding the poles of the 3-sphere behind black/white hole event horizons is a good way to change the topology to the desired one. This is in line with Mellor and Moss's ([14]) physical interpretation of the extended RNdS spacetime as containing black/white holes at the poles of the de Sitter 3-sphere. In much of the literature the statement is made that there are two *black* holes (more precisely apparently no distinction is made between black holes and white holes). We will show that different spacelike slices in the same domain can cut a future horizon (BH) and/or a past horizon (white hole). In [41], Brill interprets these event horizons as wormhole mouths at the antipodal points of the large de Sitter universe.

To further clarify Mellor and Moss's interpretation [14], consider the RNdS spacetime given by  $|Q| = M$ . As in the  $a = M$  case in KdS,  $|Q| = M$  in RNdS with  $\Lambda > 0$  is not extremal in the sense of yielding zero surface gravity for the black hole (i.e.  $r_+ = r_-$ ). For  $0 < M^2\Lambda < 3/16$ , the spacetime has three horizons. At  $M = M_{crit} \equiv (3/16\Lambda)^{1/2}$ , the outer event horizon and the cosmological horizon merge, thus yielding a degenerate cosmological horizon accompanying the inner Cauchy horizon at  $r = r_-$  (see eg. Fig 1 of [36]). For  $M > M_{crit}$ , the spacetime has only the cosmological horizon and naked singularities (see [29], [30], [41] for details and Penrose diagrams of these separate cases). Such solutions thus present potential violations of the cosmic censorship conjecture of Penrose [40]. The issues of cosmic censorship violation are not the main focus of this article so we postpone our discussion to the end of section V. More details can be found in [30], [41] and [42].

In static coordinates the RNdS metric for the  $|Q| = M$  case looks like

$$ds^2 = -f dt^2 + f^{-1} dr^2 + r^2 d\Omega_2^2, \quad (39)$$

where we now have

$$f = \left(1 - \frac{M}{r}\right)^2 - \frac{\Lambda}{3}r^2. \quad (40)$$

As before, the horizons are located at  $f = 0$  and there is a curvature singularity at  $r = 0$ .

Because static coordinates break down at the horizons [43], it is more useful to look at the RNdS spacetime with another set of coordinates (chart). Such a chart is given by *cosmological* coordinates that smoothly cover the entire region from  $r = 0$  to  $r = \infty$ . A version of various charts covering different regions of de Sitter spacetime is presented in detail in [11].

The  $|Q| = M$  RNdS metric can be written in terms of these cosmological coordinates [35]. The metric in the new coordinates is given by

$$ds^2 = -\frac{d\tau^2}{U^2} + U^2(dR^2 + R^2d\Omega_2^2), \quad (41)$$

where

$$U = H\tau + \frac{M}{R} \quad (42)$$

in which  $H \equiv \pm(\Lambda/3)^{1/2}$  is the Hubble constant. The metric above uses the  $H > 0$  value. The coordinate transformation equations from the static coordinates  $(t, r, \theta, \phi)$  to the cosmological coordinates  $(\tau, R, \theta, \phi)$  are

$$r = H\tau R + M, \quad (43)$$

$$t = \frac{1}{H} \ln H\tau - h(r), \quad (44)$$

$$\frac{dh}{dr} = -\frac{Hr^2}{(r-M)f}. \quad (45)$$

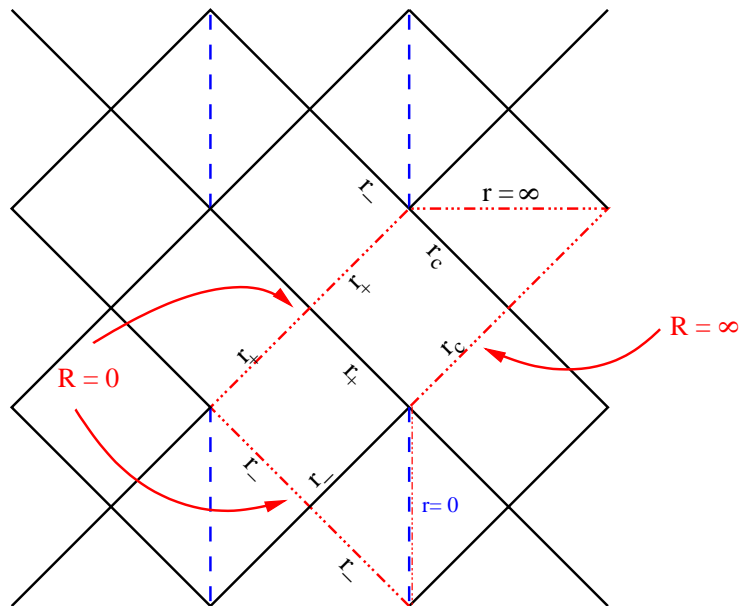


FIG. 5: Penrose diagram of the extended  $|Q| = M$  Reissner-Nordström-de Sitter spacetime. The region bounded by the 3-dotted-dashed (red) line represents a single  $(\tau, R)$  chart.  $r$  is the radial coordinate in the old static coordinates whereas  $R$  is in the new cosmological coordinates. For the  $|Q| \neq M$  generic case, a single  $\tau$  chart is not sufficient to cover the region enclosed by the red line segments (dashed-triple-dotted). Figure 5 of [29] illustrates the generic case for this coordinate chart.

It is straightforward to verify that one can go from Eq.(39) to Eq.(41) using this coordinate transformation. The curvature singularity is located at  $U = 0$  i.e.  $H\tau R = -M$ . The event horizon  $r_+$  is at  $(\tau, R) = (\infty, 0)$ , the cosmological horizon  $r_C$  is at  $(\tau, R) = (0, \infty)$  and the inner horizon  $r_-$  is at  $(\tau, R) = (-\infty, 0)$ . The details of how these values come about are explained thoroughly in [37]. In fact, one could do the same coordinate transformation from static to cosmological coordinates for the regular de Sitter spacetime. This is done in [41] explicitly and the procedure parallels the one we have outlined above.

One advantage of switching to cosmological coordinates is that a single  $(\tau, R)$  chart now covers four  $(t, r)$  charts ranging from  $r = 0$  to  $r = \infty$  and encompassing all three horizons. The boundaries of this chart are the singularity, the past inner horizon  $r_-$ , the future event horizon  $r_+$ , the past cosmological horizon  $r_C$  and the future conformal infinity at  $r = +\infty$ . Fig. 5 illustrates the region that a single  $(\tau, R)$  chart covers against the backdrop of the extended RNdS spacetime. It should be noted that for the generic  $|Q| \leq M$  case, a single  $\tau$  chart is not sufficient to cover the region shown in Fig. 5. A ‘lense-shaped region’ [29] in between  $R_{\pm} = M \pm \sqrt{M^2 - Q^2}$  would remain *uncovered* by the cosmological coordinates. More on this can be found in [29] and [41].

A few words should be mentioned about the nature of the singularity in this coordinate system. Since  $H, M > 0$  and the singularity is located at  $U = H\tau + M/R = 0$ , it exists only for  $\tau < 0$ . That is, there is no curvature singularity for  $\tau > 0$ ; for positive values of  $\tau$ , the  $\tau = \text{constant}$  hypersurfaces are regular. These non-singular surfaces are asymptotically flat as  $R \rightarrow \infty$  and they have a throat-like cylindrical geometry near  $R = 0$ , which can be seen by considering the metric of Eq.(41) at some  $\tau = \text{constant}$  slice, near  $R = 0$ . This 3-dimensional line element reads

$$dl^2 = \frac{M^2}{R^2} dR^2 + M^2 d\Omega_2^2. \quad (46)$$

This is the metric of an infinitely long throat with cross-sectional area  $4\pi M^2$ . At  $\tau = 0$ , the spatial metric is still regular and looks like Eq.(46) everywhere. As  $\tau$  is rewound to negative values starting with  $0^-$ , a singularity forms at  $R = \infty$  and as  $\tau \rightarrow -\infty$ , the singularity moves in closer with ever decreasing values of  $R$  and truncates the 3-cylinder more and more. The spacetime shrinks to a point at  $\tau = -\infty$ . Instead of going backward in time, if we simply fast-forward, we see that what we have is a spacetime that expands out of a single singular point. Because of this property, the  $(\tau, R)$  chart with  $H > 0$  is called the *expanding* chart and usually is labelled by  $(\tau_+, R)$ . From a physical perspective, this agrees with our choice of the positive root for  $H = \pm(\Lambda/3)^{1/2}$ .

There is a *companion* chart to the expanding chart that covers another equal size section of the RNdS spacetime.

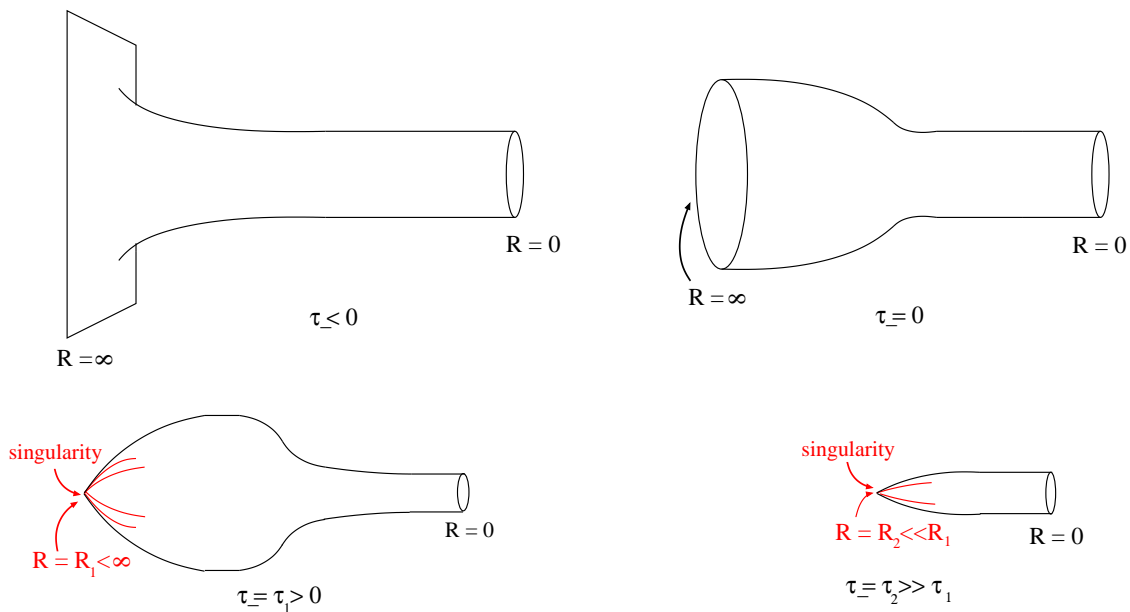


FIG. 6: Time evolution of a contracting  $(\tau_-, R)$  chart [30]. The singularity forms at  $(\tau_-, R) = (0, \infty)$  and grinds the space down as  $\tau_-$  increases tending to  $R = 0$  at  $\tau_- \rightarrow \infty$ . The Penrose diagram corresponding to this process is presented in Fig. 7. The contracting chart is the region to the left of the blue dashed line. As can be seen from the figure, at early times ( $\tau_- < 0$ ), there is no singularity, which then forms at  $\tau_- = 0$  and proceeds to grind the spacetime down for  $\tau_- > 0$  until there is nothing left but the Big Crunch itself.

This chart is called the *contracting* chart and labelled by  $(\tau_-, R)$ . The metric of Eq.(41) now is written with

$$U = H\tau_- + \frac{M}{R} = -|H|\tau_- + \frac{M}{R}, \quad (47)$$

with the negative root of  $H$  chosen. Because  $\tau$  enters the metric Eq.(41) only in the combination  $H\tau$  the  $(\tau_-, R)$  chart is actually the time reversed version of the expanding chart. The threshold moment is again  $\tau_- = 0$ , but this time the singularity forms at  $R = \infty$  as  $\tau_-$  becomes positive since at  $U = 0$ , one has  $|H|\tau_- = M/R$ . This obviously only holds true for positive values for  $\tau_-$ . As  $\tau_-$  increases, the singularity approaches ‘in’ from  $R = \infty$  and the entire spacetime collapses to a singularity at  $R = 0$  as  $\tau_- \rightarrow \infty$  (See Fig. 6 [30] for an illustration of how the spatial hypersurfaces evolve). Clearly, things happen in the  $\tau_-$  chart in the exact opposite order of the way they happen in the  $\tau_+$  chart. A similar version of these expanding/contracting cosmological charts were constructed for de Sitter spacetime by Brill in [41]. Of course there, one has no curvature singularity at  $U = 0$ .

The  $\tau_{\pm}$  charts together cover a large portion of the extended RNdS spacetime. Fig. 7 displays both of these charts in the Penrose diagram of RNdS. The black hole event horizon  $r_+$  is given by  $(\tau_{\pm}, R) = (\pm\infty, 0)$ . The cosmological horizon  $r_C$  is located at  $(\tau_{\pm}, R) = (0, \infty)$ . Since both  $\pm$ metrics give  $U = M/R \rightarrow 0$  at  $r = r_C$  (i.e.  $\tau_{\pm} = 0$ ), they can be isometrically identified, i.e. glued together. This is shown more clearly in Fig. 8. Furthermore, this identification i.e. gluing a  $+$ chart to a  $-$ chart repeats itself ad infinitum in the horizontal direction.

It can be seen from Fig. 7 that timelike lines to the “left” of the stitching boundary  $r_C$  must all go through the left-hand boundary at  $r = r_+$ , whereas timelike lines in the region to the right of  $r_C$  all emanate from the right-hand  $r_+$ . We find that in the literature, the objects beyond the two horizons at  $r = r_+$  are simply referred to as black holes, but in reality the question of which kind of hole one has depends on the type of spacelike hypersurface one is in. This is illustrated in detail in Fig. 9. We see that depending on the hypersurface chosen, the global geometry can be given by any one of the four  $BH - BH, WH - BH, BH - WH, WH - WH$  combinations. Regardless of their nature, these holes are located at the poles of the de Sitter 3-sphere. When patched together in this way there is a global time coordinate  $\tau$  which covers most of the pasted patch, and which increases “upward” in the resulting pasted spacetime, even though  $\tau_-$  decreases as  $\tau$  (and  $\tau_+$ ) increase. Because the  $\tau_-$  patch is identical to the  $\tau_+$  patch evolving oppositely in terms of a global observer, to such an observer there is a (formal) time reversal between them, so the electric fields (hence the electric charges) are reversed. (The components of the Maxwell tensor transform as  $F^{0i} \rightarrow -F^{0i}$ .) Electric field lines leaving one black hole will enter the other one at the opposing antipodal point. This is precisely Wheeler’s “charge without charge”. If desired, one could further identify the black hole throats (horizons) with each other and turn the  $S^2 \times R^1$  topology into a  $S^2 \times S^1$  topology. This identification would transform the



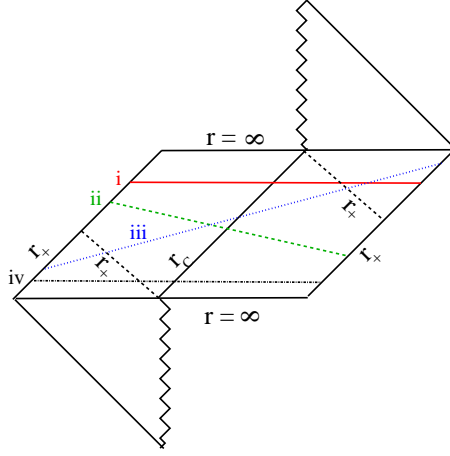


FIG. 9: Very similar to the slicing of SdS spacetime shown in Fig. 2. We use the same color coding and line types as before: Red, solid (i); green, dashed (ii); blue, dotted (iii); black, dash-triple-dotted (iv). These slices intersect BH/WH at  $45^\circ$  lines marked  $r_+$  (either solid or dotted). These slicings respectively give  $BH - BH, BH - WH, WH - BH, WH - WH$  pairings within the chosen hypersurface.

### B. Kerr-de Sitter from Reissner-Nordström-de Sitter

We will now demonstrate that the extended KdS manifold can be viewed as a 3-sphere containing a black hole at one pole and another at the opposite pole. In section IV A, we showed this concretely for the RNdS spacetime. Here, we will show that the same interpretation holds for KdS. Although this may be obvious to some (especially since Reissner-Nordström and Kerr share the same causal structure), we will still take the time to make the connection more clear. Our results to this end will not be analytically exact, but are based on a simple distortion of RNdS spacetime in which the KdS spacetime outside the event horizons remains free of singularities and other kinks. Our specific example is the very restricted case of  $a = M$  Kerr-de Sitter, but we argue that it is representative of the larger family of KdS solutions.

Ideally, we would like to find an exact coordinate transformation that would turn the KdS metric to a single black hole KT metric of Eq.(41). The KdS metric of Eq.(12) is rather complicated, so finding such a coordinate transformation has thus far been elusive. Instead, we make the KdS metric resemble the RNdS metric of Eq.(41) and use the already available coordinate transformation introduced in section IV A. To this end, we first take a  $\theta = 0$  polar cut of the metric in Eq.(12) (due to axisymmetry  $\phi$  can be set to equal any value from 0 to  $2\pi$ ). Then, in analogy to the  $|Q| = M$  RNdS case, we focus our attention solely on the  $a = M$  KdS solution. We do this so that we can rewrite  $\Delta_r$  of Eq.(13) as follows

$$\begin{aligned} \Delta_r &= r^2 - 2Mr + a^2 - \frac{\Lambda r^2}{3}(r^2 + a^2), \\ &= (r - a)^2 - \frac{\Lambda r^2}{3}(r^2 + a^2). \end{aligned} \quad (48)$$

Furthermore, we define a new time coordinate  $T$  by

$$T \equiv \frac{t}{1 + \frac{\Lambda}{3}a^2}. \quad (49)$$

This is simply a rescaling of the time coordinate by a constant factor. Putting all the new changes together into our  $a = M$  KdS metric, we obtain

$$ds^2 = - \left[ \left( \frac{r - a}{\sqrt{r^2 + a^2}} \right)^2 - \frac{\Lambda r^2}{3} \right] dT^2 + (-g_{TT})^{-1} dr^2, \quad (50)$$

where  $g_{TT}$  equals the expression inside the large square brackets. This looks very similar to the extremal RNdS metric given by Eq.(39), which we display one more time (with  $a$  replacing  $M$  for the sake of making the comparison easier to see):

$$ds^2 = - \left[ \left( 1 - \frac{a}{r} \right)^2 - \frac{\Lambda r^2}{3} \right] dt^2 + (-g_{tt})^{-1} dr^2. \quad (51)$$



We know that Eq.(51) corresponds exactly to the single mass Kastor-Traschen solution which can be covered by two charts  $(\tau_{\pm}, R)$ . We have also shown that the part of the extended RNdS covered by these two KT charts can be physically interpreted to be the de Sitter 3-sphere with black/white holes at its poles. The extremal KdS metric of Eq.(50) is very nearly identical in form to the extremal RNdS of Eq.(51). Let us see if we can massage the KdS metric (50) further to make it look more like Eq.(51). We start by defining a new coordinate  $\bar{r}$  in  $a = M$  KdS spacetime by the following:

$$\bar{r}^2 \equiv r^2 + a^2 \rightarrow \bar{r} d\bar{r} = r dr. \quad (52)$$

Since the maximum value of  $a$  is only slightly above unity (see section III), we have  $a^2/M^2 \sim \mathcal{O}(1)$ . For  $r/M \gg 1$ ,  $r \approx \bar{r}$ . The new coordinate substitution also yields the following expressions:

$$dr^2 = \frac{\bar{r}^2}{r^2} d\bar{r}^2 = \frac{\bar{r}^2}{\bar{r}^2 - a^2} d\bar{r}^2 \equiv (1 + \delta_1) d\bar{r}^2, \quad (53)$$

$$\left( \frac{r - a}{\sqrt{r^2 + a^2}} \right) = \left( \frac{\sqrt{\bar{r}^2 - a^2}}{\bar{r}} - \frac{a}{\bar{r}} \right) \equiv \left( (1 - \delta_2) - \frac{a}{\bar{r}} \right), \quad (54)$$

where

$$\delta_1 = \frac{a^2}{\bar{r}^2 - a^2}, \quad (55)$$

$$\delta_2 = 1 - \frac{\sqrt{\bar{r}^2 - a^2}}{\bar{r}}. \quad (56)$$

Above, instead of Taylor expanding in powers of  $\bar{r}$  we have simply gathered all the troublesome terms under the ‘deviation’ terms  $\delta_1$  and  $\delta_2$ . Let us first redisplay the KdS metric of Eq.(50) with these new substitutions:

$$ds^2 = - \left[ \left( (1 - \delta_2) - \frac{a}{\bar{r}} \right)^2 - \frac{\Lambda}{3} (\bar{r}^2 - a^2) \right] dT^2 + \frac{(1 + \delta_1)}{(-g_{TT})} d\bar{r}^2. \quad (57)$$

Recalling our dimensionless tilde notation, we have  $\tilde{a} = \tilde{a}^2 = 1$ . Because of this, the deviations  $\delta_1$  and  $\delta_2$  only grow to significant values near  $\tilde{r} = 1$ . For example, even for  $\tilde{r} = 2$ , the deviations do not exceed 30%. Furthermore, as  $a = M$  is not the maximum value for the spin of a Kerr black hole in de Sitter background ( $\tilde{a}_{max} \approx 1.1$ ), the actual outer black hole horizon  $\tilde{r}_+ (= r_+^2 + a^2)$  lies outside  $\tilde{r} = M$ . Since the conformal domain of interest is between the outer horizon  $r_+$  ( $\tilde{r}_+$ ) and the cosmological horizon  $r_C$  ( $\tilde{r}_C$ ) having a value for the spin less than the maximum ( $a = M < a_{max}$ ) guarantees that we are safe from the  $\tilde{r} = a$  pole in  $\delta_1$  shown in Eq.(55). For example, for value of  $\tilde{\Lambda} = 0.001$  with  $\tilde{a} = 1$  we have

$$\tilde{r}_+ \approx 1.02 \rightarrow \tilde{\tilde{r}}_+ \approx 1.5. \quad (58)$$

Both of these are larger than 1. And obviously  $\tilde{r}_+ = 1$  only at the  $\Lambda = 0$  limit. Even with such a small value (close to 0) for  $\Lambda$  the deviations do not exceed order unity; e.g. for  $\tilde{\tilde{r}}_+ = 1.5$  one has  $\delta_1 = 0.8$  and  $\delta_2 = 0.25$ .

Although one could argue that the deviation factors are large enough to be significant near the black hole horizon ( $\delta_1 \sim \tilde{r}_+ \sim \mathcal{O}(1)$ ), this does not alter the conformal structure of the spacetime in a serious manner. The deviations are contributions to the metric only near the black hole horizon (both  $\delta_1$  and  $\delta_2 \rightarrow 0$  as  $\tilde{r} \rightarrow \infty$ ). As such, they only change measurement of lengths in the vicinity of the event horizons. However, rescaling lengths by at most a factor of  $\sim 1.8$  (for  $\tilde{\tilde{r}}_+ \approx 1.5$ ,  $1 + \delta_1 \approx 1.8$ ) is not a significant change to the global structure of a given spacetime manifold. As long as we do not poke any new holes in the manifold, the general conformal picture should not change. This is the basis for our argument that the general picture of the global structure of Kerr-de Sitter should look like that of Reissner-Nordström-de Sitter. In short, even though KdS metric can not be made to look exactly like the KT metric of Eq.(41), the 3-dimensional  $\theta = 0$  sub-spacetime of  $a = M$  KdS looks very much like the  $Q = M$  RNdS metric. This resemblance is exact in the large  $r$  limit. Near the black hole horizons, the lengths are rescaled by nearly a factor of two at most, but this is not a significant change to the global structure of the KdS manifold.

As one has two oppositely charged anti-podal black/white holes in the extended RNdS spacetime, here we expect to have counter-rotating holes at the anti-podal points. The  $\tau_-$  chart runs backward with respect to the  $\tau_+$  chart (see Fig. 7) so one hole rotates oppositely to the other, therefore yielding zero net angular momentum for the extended solution. The right hand figure in Fig. 8 illustrates the physical picture for the spatial hypersurfaces.

## V. CONCLUSION

We presented a detailed look into Carter’s Kerr-de Sitter spacetime, which is the uncharged, rotating black hole solution to Einstein’s equation with cosmological constant  $\Lambda$ . As is known and was shown here, the  $a = M$  case does not yield an extremal black hole in this spacetime. We quantified this by explicitly solving the apparent horizon equation for real roots and showing that the black hole spin tops out around  $a \approx 1.1M$ . Fig. 3 demonstrates that for any  $\Lambda > 0$ ,  $a_{max} > M$ , and if  $\Lambda > 1/9M^2$  then  $a$  cannot be zero. Furthermore, if  $\Lambda$  is larger than some maximum value  $\bar{\Lambda} \approx 0.1778/M^2$  then there is no longer a black hole in the spacetime. The cosmic expansion tears the black hole apart. As far as we know, no one has published computational these results before.

We also investigated the global structure of the extended solution by first looking at the correspondence between the  $|Q| = M$  Reissner-Nordström-de Sitter and Kaster-Traschen spacetimes. Globally, the RNdS spacetime can be viewed as a 3-sphere containing oppositely charged black/white holes at its poles. In more detail, we saw that depending on the kind of spacelike hypersurface, one can get one of the four possible combinations of  $BH - BH$ ,  $BH - WH$ ,  $WH - BH$ ,  $WH - WH$  at the poles. Using a coordinate transformation and an approximation scheme, we massaged the  $a = M$  case of KdS to look very much like  $|Q| = M$  RNdS and exactly identical to it in the large  $r$  limit. This and the fact that the  $\theta = 0$  cut of KdS and RNdS have the same Penrose diagrams led us to conclude that KdS has a very similar global structure to RNdS. In this case, the physical picture (spatially) is that of a 3-sphere with a Kerr black (or white) hole at each pole; the Kerr holes counter-rotate. The holes are causally disconnected: spacelike separated in a nonsingular coordinate patch. In our description the two hemispheres of the 3-sphere are covered by a coordinate system made up of two separate natural coordinate charts and there is a natural stitching boundary at the null surface  $r_C$ . A very simple example of this stitching is given by Brill in [41] who stitches forward/backward evolving de Sitter universes (no holes) at the cosmological horizon.

Other matters not yet addressed relating to KdS spacetime include the frame dragging by the spin of the black holes, and issues with possible violation of the cosmic censorship conjecture ([40]) in this spacetime for the non-generic cases. In [29] and [30], the singularity structure of RNdS spacetime is investigated in detail. In [29], the possible naked singularities are classified under names like “generic naked singularity” or “extreme naked singularity” depending on which roots of  $f(r)$  in Eq.(36) are degenerate. The generic singularity case yields  $S^2 \times R^1$  topology for the  $t = constant$  spatial hypersurfaces. As before, we can take this to be a 3-sphere minus the poles. But whereas before the poles were cloaked behind horizons, now they are simply punctures on the 3-sphere. Since the time coordinates of the hemispheres are time reversals of each other, the punctures at the poles in RNdS act like oppositely charged point particles. Although these points are eternal naked singularities, [37] points out that these singularities do not form from an initial compact spatial hypersurface (proper initial data) thus obey a form of weak cosmic censorship. Wald also agrees with this in [42], but does not rule out the possibility of RNdS or KdS potentially providing evidence against strong cosmic censorship.

The case of “extreme naked singularity” is more interesting because the RNdS Penrose diagram suggests the creation and annihilation of a pair of point charges (with total net charge equaling zero of course, see Fig.1(d) of [29] and/or Fig.2 of [30]). These singularities have nonsingular spacelike surfaces to their past i.e. they develop from regular initial conditions. Moreover, these singularities are visible from  $\mathcal{I}^+$ . However, as shown in [30], one can find complete timelike geodesics along which the observer spends an infinite amount of proper time travelling and never sees the singularities. According to [30], these singularities then are not really ‘naked’ because they are not visible to all observers originating from a point on a regular spatial hypersurface in the past. These difficulties arise from the fact that there is no clear, universally-agreed-upon definition for naked singularities when the cosmological constant is non-zero and there is no asymptotic flatness. These interesting topics are beyond the scope of this article so we will not say more about them here.

As our work shows, the Kerr-de Sitter solution has interesting properties and comes with some puzzling peculiarities. Although at first, some of these might seem trivial, a closer look shows that they are anything but. We hope that we brought some clarity to this picture and helped the reader to have a better understanding of the Kerr-de Sitter spacetime.

## VI. ACKNOWLEDGEMENTS

S.A. thanks Leor Barack and David Garfinkle for useful suggestions and physical insights. He also acknowledges support from STFC through Grant No. PP/E001025/1.

### Appendix A: Regularity of the Axis

In section III, we noted that the factor of  $\Xi = 1 + \Lambda a^2/3$  was needed to avoid conical singularities near the black hole axis. Here, we demonstrate the role this factor plays. We look at the metric on a section of a spheroid in the vicinity of its ‘poles’  $\theta = 0, \pi$ . Near  $\theta = 0$ ,  $\sin \theta \approx \theta \ll 1$  and  $\cos \theta \approx 1$ . Furthermore, for finite  $r$ ,  $r \sin \theta$  is also small. The relevant part of the metric is

$$d\Omega_2^2 = g_{\theta\theta} d\theta^2 + g_{\phi\phi} d\phi^2. \quad (\text{A1})$$

From Eq.(12), near the pole we have

$$g_{\theta\theta} = \frac{r^2 + a^2 \cos^2 \theta}{1 + \frac{\Lambda}{3} a^2 \cos^2 \theta} \approx \frac{r^2 + a^2}{1 + \frac{\Lambda}{3} a^2}, \quad (\text{A2})$$

and

$$\begin{aligned} g_{\phi\phi} &= \frac{\Delta_\theta \sin^2 \theta}{\rho^2 \Xi^2} (r^2 + a^2) - \frac{\Delta_r a^2 \sin^4 \theta}{\rho^2 \Xi^2}, \\ &\approx \frac{\Delta_\theta \sin^2 \theta}{\rho^2 \Xi^2} (r^2 + a^2), \\ &\rightarrow \frac{\sin^2 \theta}{r^2 + a^2} \frac{1 + \frac{\Lambda}{3} a^2}{(1 + \frac{\Lambda}{3} a^2)^2} (r^2 + a^2)^2 = \frac{r^2 + a^2}{1 + \frac{\Lambda}{3} a^2} \sin^2 \theta. \end{aligned} \quad (\text{A3})$$

Above, we made use of the approximation that  $\sin^4 \theta \ll \sin^2 \theta$ . The 2-metric of Eq.(A1) becomes

$$d\Omega_2^2 \rightarrow \frac{r^2 + a^2}{1 + \frac{\Lambda}{3} a^2} (d\theta^2 + \sin^2 \theta d\phi^2). \quad (\text{A4})$$

This is the line element on a sphere in the vicinity of its poles. As can be seen from the 2-metric in Eq.(A4), the factor of  $\Xi$  effectively rescales the coordinate radius. For example, the circumference of a circle near the poles now equals  $2\pi\sqrt{r^2 + a^2}(1 + \frac{\Lambda}{3}a^2)^{-1/2} \sin \theta$  as opposed to just  $2\pi\sqrt{r^2 + a^2} \sin \theta$  for a Kerr black hole with  $\Lambda = 0$ . From a physical perspective, this type of disagreement with the Kerr result should be expected. For starters, the extra factor depends on the cosmological constant  $\Lambda$ ; and  $\Lambda$  should have an effect on the size of the black hole. If  $\Lambda$  is large, then the black hole would have to be smaller in size in order to keep itself together against the cosmic repulsion. The  $\Xi^{-1/2}$  dependence of the circumference indicates this reaction.  $\Lambda = 0$  gives  $\Xi = 1$  which corresponds to the regular Kerr case where we have the usual horizon areal radius  $(r_+^2 + a^2)^{1/2}$ . As  $\Lambda$  grows,  $\Xi$  exceeds 1, thus making the horizon radius smaller than its Kerr value. Basically, a black hole in a de Sitter universe always has to be smaller than its Minkowski counterpart in order to hold itself together against the  $\Lambda$  driven expansion that increases for larger  $r$ .

### Appendix B: Surface Gravity of the Kerr-de Sitter Black Hole

As in the Kerr case, we find a vector field  $\xi^\mu$  that is a geodesic, Killing, tangent to and regular at the event horizon. If all four conditions are satisfied then the surface gravity  $\kappa$  of the black hole is given by the following:

$$\xi^\mu \nabla_\mu \xi_\alpha |_{EH} = \kappa \xi_\alpha |_{EH}, \quad (\text{B1})$$

where  $EH$  implies that we must evaluate the equations on the event horizon. Using Killing’s equation  $\nabla_\alpha \xi_\beta = -\nabla_\beta \xi_\alpha$ , Eq.(B1) can be rewritten as

$$-\frac{1}{2} \nabla_\mu \xi^2 |_{EH} = \kappa \xi_\mu |_{EH}. \quad (\text{B2})$$

The Killing vector tangent to the event horizon of the Kerr-de Sitter black hole looks very much like its Kerr counterpart (see [34] for a comparison). In Boyer-Lindquist like coordinates of KdS spacetime,  $\xi$  is as follows ([31]):

$$\xi = \Xi \frac{\partial}{\partial t} + \Omega_H \frac{\partial}{\partial \phi}, \quad (\text{B3})$$

where

$$\Omega_H = \frac{a \Xi}{r_+^2 + a^2} \quad (\text{B4})$$

is the event horizon angular velocity. Written in Kerr-Schild like coordinates the Killing vector becomes

$$\xi = \frac{\partial}{\partial \tau} + \frac{a}{r_+^2 + a^2} \left(1 - \frac{\Lambda}{3} r_+^2\right) \frac{\partial}{\partial \Phi}. \quad (\text{B5})$$

One can readily check that  $\xi$  is null on the horizon i.e.  $\xi^2|_{r=r_+}$ . To use the geodesic equation B2 properly, we must use the global form of  $\xi^\mu$  where  $r_+$  is left as radial coordinate variable  $r$ . After all,  $\xi^\mu$  is required to be Killing only on the event horizon. We can compute the left hand side (LHS) of Eq.(B2) in any coordinate frame we wish. Using BL coordinates we get

$$\xi^2 = -\frac{\rho^2}{(r^2 + a^2)^2} \Delta_r. \quad (\text{B6})$$

Here  $\Delta_r$  and  $\rho^2$  have the usual meanings from section III. This expression is a function only of the radial coordinate  $r$ , so the only non-zero contribution to the LHS of Eq.(B2) comes from  $\nabla_r = \partial_r$  component:

$$-\frac{1}{2} \nabla_\mu \xi^2|_{EH} \longrightarrow -\frac{1}{2} \partial_r \xi^2|_{r=r_+} = \frac{1}{2} \frac{r_+^2 + a^2 \cos^2 \theta}{r_+^2 + a^2} \Delta'_r(r_+). \quad (\text{B7})$$

Above, the prime indicates differentiation with respect to  $r$  and we used the fact that  $\xi^2$  is a scalar. After taking the derivative, we evaluate everything at  $r = r_+$ . On the right hand side of Eq.(B2), we have  $\xi_\mu$ , which has a non-zero  $r$ -component because in KS coordinates, the metric has a  $g_{\tau r}$  crossterm. Thus, we have

$$\xi_r = \frac{2Mr\rho^2}{(r^2 + a^2)^2(1 - \lambda r^2)}. \quad (\text{B8})$$

Now, Eq.(B2) becomes

$$\frac{1}{2} \frac{\rho_+^2}{(r_+^2 + a^2)^2} \Delta'_r(r_+) = \kappa \frac{2Mr_+\rho_+^2}{(r_+^2 + a^2)^2(1 - \lambda r_+^2)}, \quad (\text{B9})$$

which gives for  $\kappa$

$$\kappa = \frac{1 - \frac{\Lambda}{3} r_+^2}{4Mr_+} \Delta'_r(r_+), \quad (\text{B10})$$

consistent with Eq.(26) above. Eq.(B10) precisely matches the expression presented in different notation in [31].

### Appendix C: Kastor-Traschen Spacetime

First discovered by Kastor and Traschen ([35]), the KT metric represents a de Sitter universe containing  $N$  black holes, each located at  $\mathbf{R}_i$ . For  $H \equiv (\Lambda/3)^{1/2}$ , the KT metric is given to be:

$$ds^2 = -\frac{d\tau^2}{U^2} + U^2(dR^2 + R^2 d\Omega_2^2), \quad (\text{C1})$$

where

$$U = H\tau + \sum_{i=1}^N \frac{M}{|\mathbf{R} - \mathbf{R}_i|}. \quad (\text{C2})$$

This is the same metric as that of  $|Q| = M$  RNdS spacetime except with more than one black hole. Physically, this represents the situation in which the Coulomb force cancels the Newtonian gravity and the black holes accelerate away from each other under the influence of the cosmic expansion. As was shown in section IV A, the spatial geometry

near each black hole is that of a 3-cylinder. In this “expanding” coordinate system of Eq.(C1), one starts with  $N$  singularities at  $\tau = -\infty$  which then expand into smooth, non-singular spatial 3-cylinders by the time  $\tau = 0$ . For  $\tau > 0$ , we have  $N$  black holes that are smoothly joined near  $R = \infty$ . The case of a single mass corresponds to the  $|Q| = M$  RNdS metric presented in section IV A. One can also write this metric using a contracting chart.

- 
- [1] B. Carter in *Les Astres Occlus* ed. by B. DeWitt, C. M. DeWitt, (Gordon and Breach, New York, 1973).
- [2] E. Komatsu et al., *Astrophysical J. Supp.*, arxiv.org/1001.4538 (2010).
- [3] J. Dunkley et al., *Astrophysical J. Supp.*, submitted (2009).
- [4] D. N. Spergel et al., *Astrophysical J. Supp.* **170**, 377, (2007).
- [5] C. L. Bennett et al., *Astrophysical J. Supp.* **148**, 1, (2003).
- [6] A. G. Riess et al., *Astronomical J.* **116**, 1009, (1998).
- [7] S. Perlmutter et al., *Astrophysical J.* **517**, 565, (1999).
- [8] W. de Sitter, *Mon. Not. Roy. Ast. Soc.* **76**, 699, (1916).
- [9] W. de Sitter, *Mon. Not. Roy. Ast. Soc.* **77**, 155, (1916).
- [10] W. de Sitter, *Mon. Not. Roy. Ast. Soc.* **78**, 3, (1917).
- [11] S.W. Hawking, G.F.R. Ellis, *Large Scale Structure of Space-Time* (Cambridge University Press, Cambridge, 1973).
- [12] E. Schrödinger, *Expanding Universes* (Cambridge University Press, Cambridge, 1956).
- [13] F. Kottler, *Über die physikalischen Grundlagen der Einsteinschen Gravitationstheorie*, *Annalen der Physik*, **361**, 401, (1918).
- [14] F. Mellor, I. Moss, *Phys. Lett.* **B222**, 361, (1989).
- [15] H. Weyl, *Über die statischen, kugelsymmetrischen Lösungen von Einsteins "kosmologischen" Gravitationsgleichungen*, *Phys. Z.* **20**, 31, (1919).
- [16] E. Trefftz, *Das statische Gravitationsfeld zweier Massenpunkte in der Einsteinschen Theorie*, *Mathem. Ann.* **86**, 2317, (1922).
- [17] R. C. Tolman, *Relativity Thermodynamics and Cosmology*, (Clarendon Press, Oxford, 1934).
- [18] A. Ashtekar, B. Krishnan, *Dynamical Horizons and Their Properties*, arXiv.org/gr-qc/0308033, (2003).
- [19] J. Guven, D. Nuñez, *Phys. Rev.* **D42**, 2577, (1990).
- [20] G.W. Gibbons, S. W. Hawking, *Phys. Rev.* **D15**, 2738, (1977).
- [21] J.F. Plebański, M. Demiański, *Ann. Phys.* **98**, 98, (1976).
- [22] H. Stephani, D. Kramer, M. MacCallum, C. Hoenselaers and E. Herlt, *Exact solutions of Einstein's field equations*, 2nd edition, (Cambridge University Press, Cambridge, 2003).
- [23] J.B. Griffiths, J. Podolský, *Int. J. Mod. Phys.* **D15**, 335, (2006).
- [24] J.B. Griffiths, J. Podolský, *Phys. Rev.* **D73**, 044018, (2006).
- [25] S. Chandrasekhar, *The Mathematical Theory of Black Holes* (Oxford University Press, Oxford, 1983).
- [26] C. W. Misner, K. S. Thorne, and J. A. Wheeler, *Gravitation* (W.H. Freeman, New York, 1970).
- [27] B. Carter, *Commun. Math. Phys.* **17**, 233 (1970)
- [28] *Handbook of Mathematical Functions* edited by M. Abramowitz , I. A. Stegun , 1964.
- [29] D.R. Brill, S. A. Hayward, *Class. Quan. Grav.* **11**, 359, (1994).
- [30] D.R. Brill, G.T. Horowitz, D. Kastor, J. Traschen, *Phys. Rev.* **D49**, 840, (1994).
- [31] G.W. Gibbons, H. Lü, D.N. Page, C.N. Pope, *Jour. Geometry& Physics* **53**, 49, (2005), [arXiv.org/hep-th/0404008].
- [32] E. Poisson, *A Relativist's Toolkit* (Cambridge University Press, Cambridge, 2004).
- [33] M.P. Hobson, G. Efstathiou, and A.N. Lasenby, *General Relativity* (Cambridge University Press, Cambridge, 2006).
- [34] R.E. Wald, *General Relativity* (The University of Chicago Press, Chicago, 1984).
- [35] D. Kastor, J. Traschen, *Phys. Rev.* **D47**, 5370, (1993).
- [36] S.A. Hayward, K. Nakao, T. Shiromizu, *Phys. Rev.* **D49**, 5080, (1994).
- [37] K. Nakao, T. Shiromizu, S.A. Hayward, *Phys. Rev.* **D52**, 796, (1995).
- [38] J.A. Wheeler, *Geometrodynamics* (Academic, New York, NY, 1962).
- [39] S.A. Hayward, *Phys. Rev.* **D49**, 6467, (1994).
- [40] R. Penrose, *Nuovo Cimento* **1**, 252, (1969).
- [41] D. Brill, *Lecture Notes in Physics* **460**, 77, (1996), [arXiv.org/gr-qc/9501023].
- [42] R. M. Wald, talk given at the April 1997 APS Meeting in Washington, D.C., [arXiv.org/gr-qc/9710068].
- [43] This breakdown is well known in the Schwarzschild spacetime expressed in Schwarzschild coordinates.